Optical Fiber Technology 73 (2022) 103059

Contents lists available at ScienceDirect

Optical Fiber Technology

journal homepage: www.elsevier.com/locate/yofte

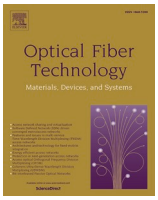

Invited Papers

# (INVITED)Investigation of liquids with microcavity in-line Mach-Zehnder interferometers – impact of the microcavity shape on the sensing performance

Tomasz Gabler [a], Monika Janik [a], Changrui Liao [b], Anna Myśliwiec [a], Marcin Koba [a,c], Martin Jönsson-Niedziółka [d], Ying Wang [b], Mateusz Śmietana [a,*]

[a] Warsaw University of Technology, Institute of Microelectronics and Optoelectronics, Koszykowa 75, 00-662 Warsaw, Poland
[b] Key Laboratory of Optoelectronic Devices and Systems of Ministry of Education and Guangdong Province, College of Physics and Optoelectronic Engineering, Shenzhen University, Shenzhen 518060, China
[c] National Institute of Telecommunications, Szachowa 1, 04-894 Warsaw, Poland
[d] Polish Academy of Sciences, Institute of Physical Chemistry, Kasprzaka 44/52, 01-224 Warsaw, Poland

ARTICLE INFO

*Keywords:*
Optical fiber sensor
Mach-Zehnder interferometer
Refractive index sensing
Femtosecond laser micromachining
Label-free biosensing
Microfluidics

ABSTRACT

In this work, we review microcavity in-line Mach-Zehnder Interferometers (μIMZI) obtained in optical fibers using femtosecond (fs) laser micromachining. These structures can be considered as a great solution satisfying the requirements mentioned above for small-volume RI sensing applicable in label-free biosensing. Furthermore, application of the femtosecond laser facilitates tailoring of the microcavity's shape with high degree of flexibility. Over the years, various μIMZI have been reported, where RI sensing has been mainly analyzed but no impact of the microcavity shape has been shown up to date. Thus, on top of the review on μIMZIs, in this work, we discuss the impact of the shape of the on the sensing performance of the device. We use two representative examples of microcavity shapes, i.e., U-shape and V-trench, made in a standard single-mode fiber. Despite different shapes, both structures offer similar and high RI sensitivity (exceeding 13,000 nm/RIU in the RI range 1.333–1.340 RIU). However, the performance of the structures in microfluidic systems is different. Based on the experimental results and numerical simulations, the advantages and disadvantages of different shapes are discussed for their application in investigations of liquids and biosensing.

## 1. Introduction

Nowadays, there is an increasing demand for highly accurate sensing solutions, particularly those for biomaterials investigations. Usually, due to low or very low amounts of the bioanalytes available for testing, the sensors should be capable of analyzing possibly low volumes. These properties are extremely desirable in the case of immunosensing based on optical fibers [1]. When optical sensing is considered, especially relying on label-free principles, such properties of the materials as refractive index (RI) and thickness of the biological film formed on the sensor surface are typically of interest. Moreover, such sensors are desired to be combined with microfluidic systems, which give control over the motion of the low volumes and therefore enhance sensor repeatability and accuracy of acquired data. A negligible interference with other environmental parameters is also highly expected.

In recent years, the optical sensors community has effectively responded to the demand for sensing solutions in various fields e.g. cancers detection [2]. Interest in fiber optic-based sensing technology has been driven by simultaneous developments in, e.g., point-of-care diagnostics [3] with a recognized need to perform rapid, accurate, and efficient on-site examinations, often on minimal sample volumes [4,5]. Some of the sensors have already been successfully combined with microfluidic systems [6–8], aiming to ensure efficiency and repeatability of the diagnostic processes, as well as their interrogation with other analyzing or supporting elements, such as, e.g., electrochemical analyzing setups, providing enhanced information about the material under examination [9].

Among others, the development of fiber optic sensors operating according to Mach-Zehnder interferometer (MZI) configuration has been observed. These sensors identify wave phase differences between two

* Corresponding author.
*E-mail address:* Mateusz.Smietana@pw.edu.pl (M. Śmietana).

https://doi.org/10.1016/j.yofte.2022.103059
Received 21 April 2022; Received in revised form 27 August 2022; Accepted 14 September 2022
Available online 24 September 2022

beams originating from one source but following different paths. The paths differ in length or optical properties, whereas the latter are of a main interest for biosensing applications. The optical fibers lead the wave in and out of the MZI and often also guide one or both the beams, where guiding conditions in one of the paths are disturbed by a measured parameter. Optical fiber interferometers can be obtained in many ways, e.g., by fiber tapers [10–13], splicing [14–16], and incorporating photonic crystal fibers [17,18], or various other types of optical fibers [19–21]. However, although all these sensors show relatively high sensitivity, such fabrication methods are often not sufficiently repeatable and usually require sample volumes exceeding hundreds of μL.

Parallel development of laser-based microfabrication techniques, especially those based on femtosecond (fs) lasers, enabled fast, precise, and repeatable processing of many materials [22,23]. In contrast to standard lasers, fs lasers offer very short impulses with high peak power. Using nonlinear effects and overcoming diffraction limits, fs lasers have become highly effective in micromachining materials. They have also played a significant role in manufacturing optical fiber-based sensors. Fiber Bragg gratings (FBGs) [24–26] and long-period fiber gratings (LPFGs) [27–29] fabricated with fs laser were used for e.g. temperature and relative humidity sensing. Micromachining has also been applied to fabricate various grooves in a side surface of the optical fiber cladding enabling direct interactions of external medium with the light guided in the fiber core. When the depth of such a groove significantly exceeds the optical fiber core diameter, its walls act as semi-transmissive mirrors for the light beam propagating through the core. Therefore, the micro Fabry–Perot (FP) interferometers [30,31] may be obtained as an effect. However, when the depth of the microcavity reaches approximately half of the optical fiber core, an in-line MZI (μIMZI) can be obtained.

In terms of μIMZI, we may distinguish between internal closed microcavities/channels, microcavities made along with additional sensing structures, and open in-fiber cavities/trenches/channels. The first group includes internal, closed air microcavities adjacent to the optical fiber made using fs laser and fusion splicing [32]. Similarly, double air cavities [33] and asymmetric variations [34] were developed. In addition, there are also structures where specially designed microchannels connect the internal air microcavity with the outside environment [35,36]. The second group of μIMZI includes sensors made with fiber tapers [37,38], fiber tapers with single [39,40] and double air cavities [41], FBGs [42], or LPFGs [43]. What is worth mentioning, this group of sensors enables multi-parameter sensing.

The third group of μIMZI includes open, D-shape [44,45], V-shape [46,47], circular U-shape microcavities [48,49] as well as advanced triple-channel configurations [50]. The fs laser micromachining of these sensing structures has in some cases been supported by post-processing based on hydrofluoric acid (HF) etching [46,51] or reactive ion etching (RIE) [52]. It aims to reduce the roughness and irregularity of the microcavity's surface, which improves the quality of the optical response and enables its precise tuning. Tailoring the response and RI sensitivity has also been done by enlarging the microcavity [53] and deposition of a thin material on its surface [54]. All these μIMZIs in addition to the typical advantages of optical fiber sensors, such as immunity to external electromagnetic interference, capability for real-time monitoring, or working in harsh environments, have gained popularity due to their high sensitivity and compact size. The possibility of obtaining low-temperature cross-sensitivity must also be noted since it is crucial for biosensing applications. Thus, MZI sensors has been widely investigated for biological research, in particular bacteria sensing [55–57], DNA amplification monitoring [58], or protein detection [36]. High temperature sensing applications [59] and combination of the μIMZIs with electrochemical measurements for optical monitoring of chemical reactions [60] have also been reported. Possible enhancement of the sensing functionalities by combining the μIMZI with LPFG [43] or fabricating microcavity in a bimodal optical fiber [61] has also been explored.

## 2. Working principle of μIMZI

Due to the high accuracy of the fs laser micromachining and supporting post-processing methods, the sensing performance of μIMZI can be tuned at the stage of the microcavity fabrication. Although all of the mentioned μIMZI structures differ in geometry, their working principle is the same. The beam propagating through the fiber core splits into two optical paths on the wall of the optical fiber microcavity. One arm of the interferometer is the microcavity itself, whereas the second one is the remaining part of the core. As a result, electromagnetic waves propagating through both arms interfere at the distant wall of the microcavity, and the interference minima are observed in the optical spectrum. At the micromachining stage, the main properties that can be adjusted are depth and length of the cavity above the fiber core region, cavity shape, which mainly concerns the shape of the cavity's upper part as an inlet/outlet for the investigated medium, and amount of material removed from the fiber cladding. In general, intensity ($I$) at the μIMZI output can be represented as in Eq. (1), where $I_{core}$ and $I_{cavity}$ are intensities of the two interfering waves, $d$ is the length of the cavity, $n_{eff}^{core} - n_{eff}^{cavity}$ is the difference in effective refractive indices for waves in the core and the microcavity, $\lambda$ is a wavelength and $\varphi_0$ is the initial phase. The microcavity depth has the major impact on the $I_{core}$ and $I_{cavity}$ i.e., the beam-splitting effectiveness followed by the minima's depth in the spectral response.

$$I = I_{core} + I_{cavity} + 2\sqrt{I_{core}I_{cavity}}\cos\left(\frac{2\pi d(n_{eff}^{core} - n_{eff}^{cavity})}{\lambda} + \varphi_0\right) \quad (1)$$

The interference pattern shows minima ($\lambda_m$) as defined in Eq. (2).

$$\lambda_m = \frac{2\pi d\left(n_{eff}^{core} - n_{eff}^{cavity}\right)}{(2m+1)\pi - \varphi_0} \quad (2)$$

The difference between two adjacent interference wavelengths, i.e., free spectral range (FSR), can be presented as in Eq. (3).

$$FSR = \lambda_m - \lambda_{m+1} = \frac{\lambda_m\lambda_{m+1}}{\left(n_{eff}^{core} - n_{eff}^{cavity}\right)d} \quad (3)$$

Such parameters as $\lambda_m$ and FSR are crucial for sensing purposes. They simply allow for observation of the minima and their evolution with a certain interrogation setup. It must also be noted that when $d$ increases, the FSR decreases, and therefore a number of minima in a certain spectral range increases. This may disturb minima finding automatization in the interrogated spectral range.

The $d$, which is the main fabrication parameter except the cavity depth, can be defined as in Eq. (4).

$$d = \frac{\lambda_m\lambda_{m+1}}{\left(n_{eff}^{core} - n_{eff}^{cavity}\right)(\lambda_m - \lambda_{m+1})} \quad (4)$$

When investigations of liquids are of interest, refractive index (RI) sensitivity ($S_{RI}$) can be defined by Eq. (5).

$$S_{RI} = \frac{d\lambda_m}{dn_{ext}} = \frac{2\pi d}{(2m+1)\pi - \varphi_0}\left(\frac{dn_{eff}^{core}}{dn_{ext}} - \frac{dn_{eff}^{cavity}}{dn_{ext}}\right) \quad (5)$$

According to Eq. (5), the $S_{RI}$ is proportional to $d$, so for highly sensitive devices, long microcavities are expected. Considering this fact, a grove in the fiber cladding should be made along the fiber core. However, ablation of a large part of the fiber induces fragility of the device. For narrow groves in turn, liquid exchange in the cavity is very limited. Thus, from the sensing performance point of view, not only the length and depth of the cavity are important, but the shape of the cavity also seems essential.

Works on application of the μIMZI for biosensing, as indicated above, have already been reported. When it operates according to label-free concept relying on RI changes on the surface of the cavity, it can be

very universal i.e., sensing properties are determined by the applied receptor. This paper discusses the impact of the μIMZI's shape on its sensing performance and functionality. We review the shapes of the fs laser micromachined microcavities reported to date and discuss the impact of the shape for two chosen representatives, i.e., narrow V-trench along the fiber, where medium-light interaction length (*d*) can be extended, and U-shape, where in turn the interacting medium exchange is more effective. For these two examples, we investigate the impact of shape and length of the microcavities on the spectral response of the sensor, and its $S_{RI}$. Furthermore, the μIMZIs underwent liquid flow simulations aiming to identify their performance when integrated with the microfluidic systems. The analysis reported in this work may be considered a guide for designing such in-fiber structures tuned towards their high performance in specific applications.

## 3. Experimental details

### 3.1. Fabrication of the microcavities

The μIMZI discussed in this work were fabricated in a side surface of standard Corning SMF28 fibers with core and cladding diameter of 8 and 125 μm, respectively, but using different experimental setups for each of the shapes. The two types of the μIMZI discussed in this work were fabricated in laboratories specialized in fabrication of these particular types of structures. The technological parameters were well-optimized for each of the structure. Some of the technical aspects of the fabrication process may be different, but they were tailored to achieve as high performance of the structures as possible.

#### 3.1.1. U-shapes

The circular U-shape microcavities with a conical inlet where external and internal diameters reached 80 μm and 60 μm, respectively, and depth 62.5 μm, were fabricated in National Institute of Telecommunications (Poland) using NKT Origami 10XP laser operating at 1030 nm. The fabrication procedure and experimental setup was similar to the one reported in [48]. The fiber was irradiated by ca. 400 fs pulses. Fused silica glass has deficient absorption at 1030 nm, and therefore linear absorption of the laser radiation does not occur when the glass is irradiated by the laser beam. The system worked with a repetition rate of 15 kHz. The laser beam was focused on the sample with a suitably designed micromachining setup based on a Newport μFab system. It was equipped with a x20 lens (NA = 0.30). The laser pulse energy was set to 6 nJ. Fiber transmission was monitored during the process with an NKT Photonics SuperK COMPACT supercontinuum white light source and a Yokogawa AQ6370D optical spectrum analyzer working with 0.5 nm resolution. The fabrication process was controlled with in-house developed software and performed under constant temperature and humidity conditions.

#### 3.1.2. V-trenches

These microcavities were manufactured in the laboratories of Shenzhen University (China) following the procedure described in Li et al. [36]. For the process, a laser with the following parameters was used: wavelength 800 nm, pulse duration 120 fs, and repetition frequency 1 kHz. The beam was focused on the fiber using x10 objective lens with a numerical aperture of 0.25. The shutter controlled the opening and closing of the laser output, and the micromachining process was observed in real-time with a CCD camera. The average laser power maintained in the target area was ~65 nJ and. The optical fiber was mounted on a triaxial computer-controlled stage with a control resolution of 40 nm. The laser beam was focused in the center of the fiber and during the micromachining process. The fiber was moved 20 μm to the side so that the focused beam did not damage the core throughout its diameter. This was the starting point for the process.

### 3.2. Microscopic analysis

The images and 3D models of the investigated microcavities were obtained using Olympus LEXT 3100 confocal microscope supported by x20 and x50 lenses. The dimensions were determined using the embedded software. It needs to be noted that the dimensions (especially height) are specified as precisely as possible, but because of non-ideals caused during manufacturing, the obtained values may be burdened with significant error. The volume of microcavities was brought closer to ideal geometric solids.

### 3.3. Optical measurements

Experimental setup for optical measurements was simple and similar to one reported in Janik et al. [48]. The spectral responses of the microcavities were measured in a wide wavelength range, i.e., from 1100 to 1700 nm, using a Yokogawa AQ6370B optical spectrum analyzer and a Leukos SM30 supercontinuum white light laser source. The RI sensitivity was measured by immersing the sensors in glycerin/water solutions, with the RI being in the range of $n_D = 1.33292–1.34025$ RIU. The $n_D$ of the solutions was determined using a Rudolph J57 automatic refractometer working with ±0.00002 RIU accuracy. The transmission measurements were conducted at constant mechanical tension and temperature (25 °C).

### 3.4. Numerical analysis

Numerical analysis made for the purpose of this work concerned electromagnetic field distribution in the device and liquid flow analysis in the microchannel.

#### 3.4.1. Electromagnetic field

The electromagnetic field distribution in the microcavity was calculated using the finite-difference time-domain (FDTD) method implemented in the Ansys/Lumerical Device Suite software similarly to the procedure described in Gabler et al. [60]. The optical fiber was modeled using a built-in cylindrical fiber structure with dimensions of a standard single-mode fiber. The RIs of the core and cladding were based on data reported in Biswas et al. [62]. The U-shape microcavity was modelled as a cylinder reaching up to 63.4 μm into the optical fiber. The V-tapered microcavity was modelled as a cuboid with the base of an equilateral triangle reaching 80 μm into the optical fiber. Both cavities were filled with an RI of 1.33 RIU. A light source covering the spectral range of 1100–1700 nm was placed inside the fiber core, 450 μm before the microcavity. Varying mesh sizes were used for calculation purposes, i.e., coarse size of 0.77–0.77–0.2 μm (along the X–Y–Z axes) in the general simulation area and fine size of 0.1–0.1–0.2 μm in the core. Diversification was introduced to achieve greater precision for intense electromagnetic fields.

#### 3.4.2. Flow analysis

Numerical analysis of the flow was performed using the Comsol 5.6 software with the laminar flow module in the way as described in Krześniak et al. [63]. The rectangular channel and geometries of the microcavities were described in 3D coordinates. The change of concentration of analyzed liquid with time was monitored at the bottom of the cavity. The angle of the cavity in the flow channel was varied to see the effect on the response time. In order to obtain the distribution of concentration and streamlines in the volume, simulations were also carried out for cross-sections in the middle part of the microcavities. The simulation was performed for 25 μl $min^{-1}$ flowrate and microcavity angles of 0°, 30°, 45°, 60°, 90°.

## 4. Results and discussion

The most common microcavities developed to obtain μIMZIs are

shown schematically in Fig. 1. Insets represent the top view of the cavity and the shape of the cavity cross-section along the optical fiber long axis. The earliest produced and described is the D-shape microcavity (Fig. 1 (A)) [45]. This type of microcavity has an open shape that allows for effective exchange of a medium (liquid or gas) and measurements of its properties. On the other hand, it is fragile and thus difficult to handle. That is why more closed shapes were proposed later. As an improved D-shape structure in terms of mechanical properties, a U-shape (cylindrical) structure can be considered (Fig. 1(B)) [48]. This structure may offer higher than for D-shape mechanical robustness at the slight expense of inferior exchangeability of the investigated medium. However, it must be noted that the diameter of the U-shape cavity is limited to approx. 80 μm. Larger diameters as in case of the D-shape one, significantly affect the mechanical properties of the structure.

Since according to Eq. (5) $S_{RI}$ of the device follows its *d,* longer cavities are expected. The solution for increasing *d* in case of the U-shape concept is to fabricate second microcavity overlapping the first one [53] or fabricate a V-shape structure along the fiber core as shown in Fig. 1(C) [46]. The *d* for the V-shape cavity can be extended to over 100 μm [46], but the structure is relatively narrow, what in turn may have an impact on effectiveness of medium exchange in the cavity. That is why, to increase the V-shape cavity volume, it can be made as a slightly off-set as shown in Fig. 1(D) forming a V-trench. Such a shift provides a sensor with a much greater depth than the typical 62.5 μm, as part of its volume bypasses the core of the fiber.

Essentially, it is only necessary to remove a certain amount of the fiber cladding to reach the core and obtain an interference pattern. As indicated above, the shape of the microcavity, highly affects other functional properties of the μIMZI. To investigate the influence of the parameters of the microcavities on their performance, the microcavities as shown in Fig. 1(B) and (D) were investigated next. It must be noted that the U-shape structure investigated in this work has a slightly conical inlet differing it from the simplified one shown in Fig. 1(B). This feature does not affect the optical response of the structure and ease the efficient and quick introduction of the measured solution into the microcavity.

In Fig. 2 microscopic images of the two types of μIMZI discussed further are shown. Their geometrical parameters are listed in Table 1. Additional images of of these structures e.g. those got with SEM can be found in Wang et al. and Janik et al. [47,53]. Geometry of the selected types of μIMZI structures was optimized and shown in Li et al. and Janik et al. [36,48]. The estimated volume of the microcavities is similar despite significant differences in the shape of the cavities. However, a broader U-shape microcavity allows for e.g., insertion of external elements such as a microelectrode and electrochemical measurements [60]. Good access to the bottom of the cavity facilitates its functionalization. and exchange of the solutions as required for label-free biosensing [55]. A V-trench in turn is narrower and deeper which does not make this shape suitable for installation of additional elements in it, but on the other hand it may be useful when long interaction length between guided light and the medium is expected.

The results of numerical calculations of the electromagnetic field distribution in the middle of the microcavity is shown in Fig. 3. In both cases, light propagates through the microcavity and residual core as indicated in the figure by the dashed lines. The microcavity edge presented in Fig. 3(A) slightly affects the field distribution. Further simulations (not shown here) indicate that reduction of the core or/and further deepening of the V-trench microcavity cause higher electromagnetic field intensities to appear in the microcavity. The interactions with a medium in the cavity do not exceed ca. 9 μm above the micromachined surface of the core. Thus, if enough amount of cladding is removed, the calculations presented in Fig. 3 can be treated as universal and applicable to various types and shapes of the cavities. The analysis shows that despite geometric differences in the microcavities, similar optical responses of the μIMZI sensors may be expected.

### 4.1. Refractive index sensing

Performance of the two cavities as RI sensors is crucial for label-free biosensing applications. The μIMZI may be used to identify the RI changes in the cavity volume, i.e., in the area where the wave interacts

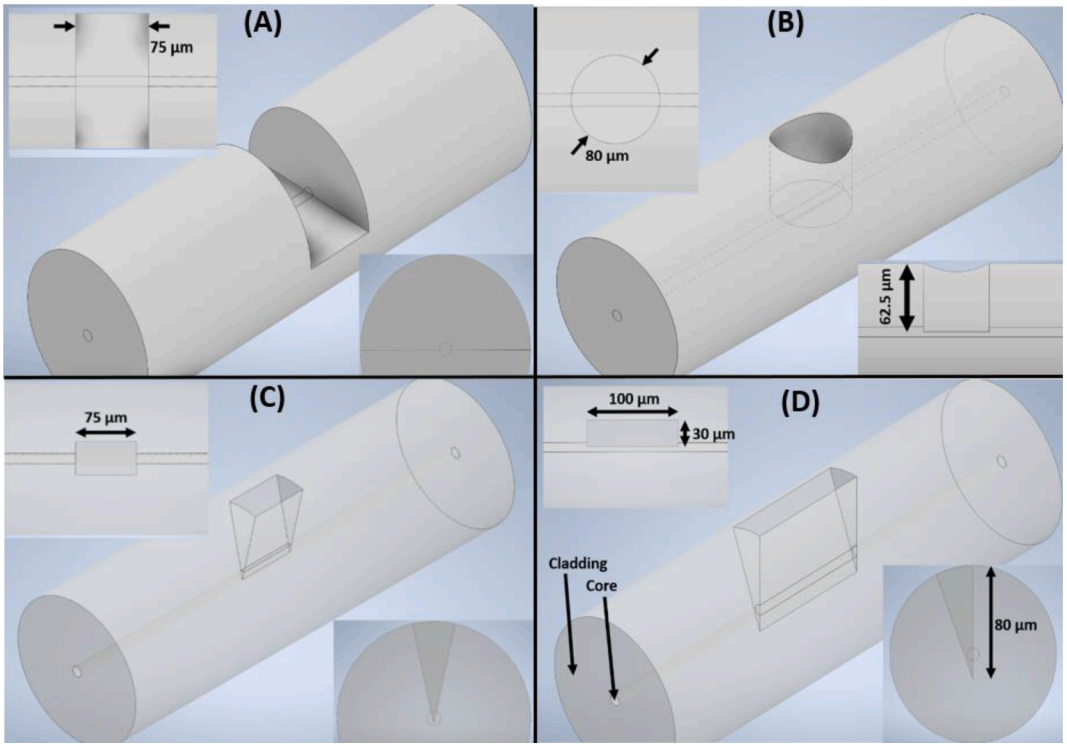


**Fig. 1.** Schematic representation of different μIMZI. D-, U-, V-shape and V-trench microcavities were shown in (A), (B), (C) and (D) respectively. Inlets represent the top view and the cross-section along the optical fiber.

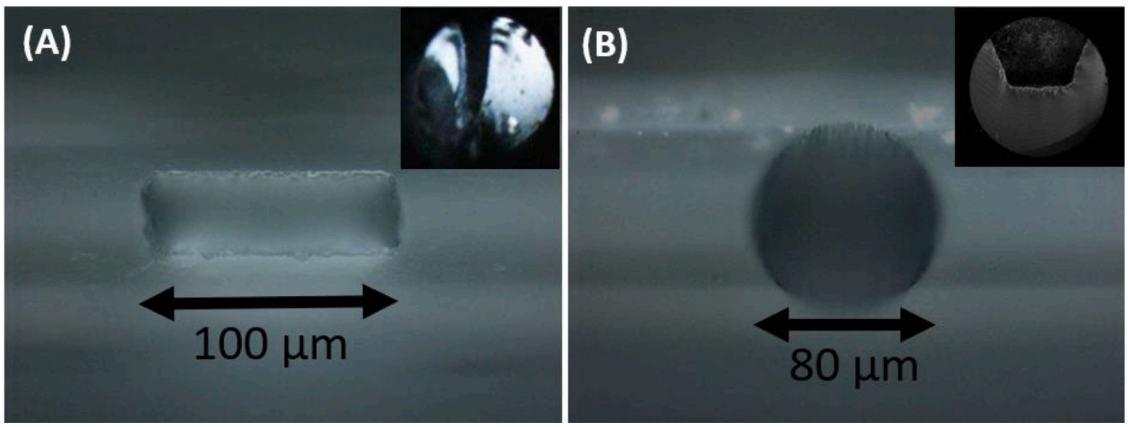


**Fig. 2.** The top-view of the V-trench (A) and U-shape (B) in-fiber microcavity considered in this work. Insets show their cross-sections.

**Table 1**
Geometrical parameters of the investigated microcavities.

| Sample | U-shape | V-trench |
|---|---|---|
| Length [µm] | 60 (diameter) | 100 |
| Width [µm] | 60 (ID), 80 (OD) | 35 |
| Height [µm] | 63 | 80 |
| Volume [pL] | 176.7 | 140 |

as shown in Fig. 3, or on the cavity bottom when a biomaterial binds to the functionalized surface [55]. The two ways of interactions may be applied for different biosensing purposes, i.e., when the RI is influenced by biomolecules suspended/floating in the cavity or gathered at its bottom surface.

It must be noted that we have performed RI sensing measurements of tens of µIMZI. Due to the high repeatability of the micromachining process with the femtosecond laser, the obtained structures have shown a high repeatability. In Fig. 4 are shown transmission spectra for the two chosen microcavities filled with aqueous solutions with RI ranging from 1.33292 to 1.34025 RIU. The transmitted power and wavelength

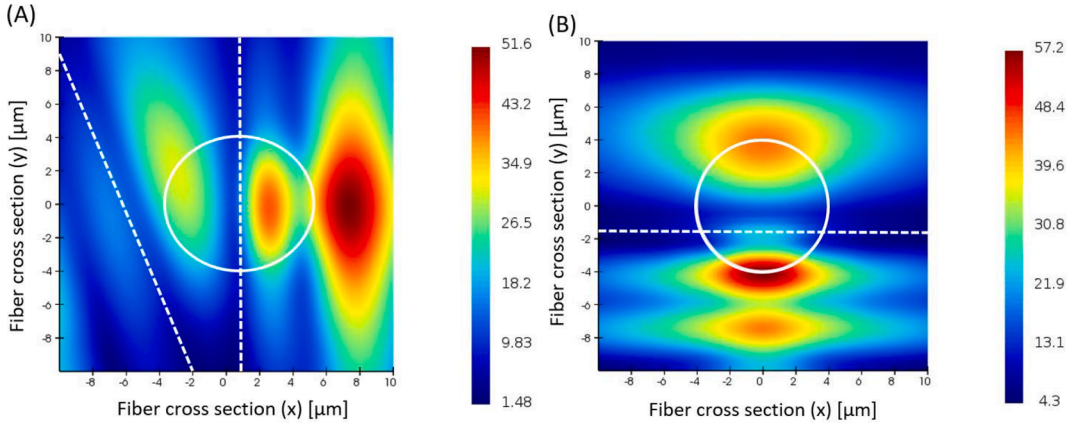


**Fig. 3.** Results of simulation presenting X-Y cross-section of an optical fiber with electromagnetic field distribution $\sqrt{|E_x^2| + |E_y^2| + |E_z^2|}$ plotted in the middle of V-trench (A) and U-shape (B) microcavity. The calculations were run for the RI filling the microcavity set to 1.33 RIU. The white solid lines and the white dashed lines represent the core of the fiber and the cavity boundaries, respectively.

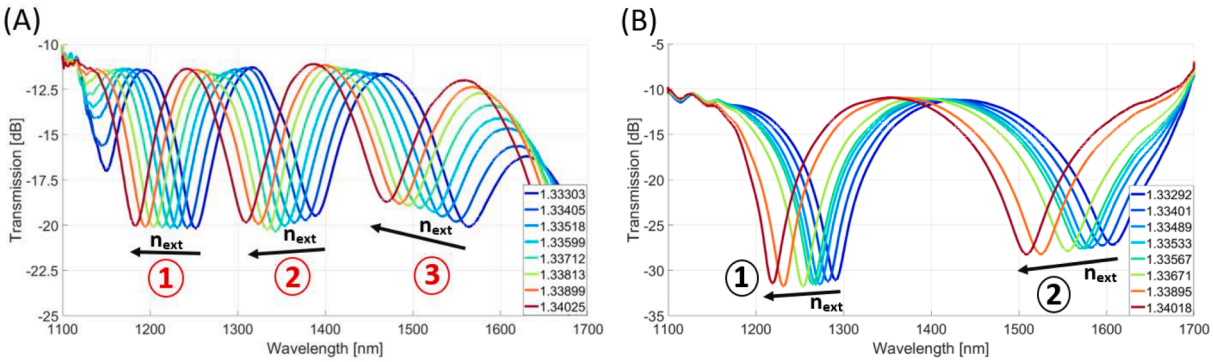


**Fig. 4.** Results of experimental analysis showing spectral response of the V-trench (A) and U-shape (B) microcavity to changes of the RI filling the microcavities.

corresponding to the interference minimum change with the RI. Due to the length of the optical path, as described by Eq. (4), in the wavelength range 1100–1700 nm there are clearly seen three interference minima in the case of V-trench (Fig. 4(A)) and two minima in the case of U-shape microcavity (Fig. 4(B)). The minima shift towards shorter wavelengths as the RI of the solution in microcavities increases which is consistent with the Eq. (2). As expected, the *d* of the microcavity is crucial for RI sensitivity and the FSR i.e., number of minima observed in the spectral range of interest. However, this example shows that the influence of the other parameters of the shape on the operation of the sensor may be secondary.

Even though insignificant and negligible deviation of measured points from approximation lines can be found, for both sensing structures the shift with RI is highly linear in the applied RI range. The U-shape microcavity shows the RI sensitivity ranging from over 10,000 nm/RIU up to almost 14,000 nm/RIU for the minimum at shorter (marked as No. 1) and longer wavelength (marked as No. 2), respectively. The V-trench microcavity, despite the different cavity shape presents comparable $S_{RI}$, which is approximately 10,000 nm/RIU for No. 1 and 2 minimum, and over 13,000 nm/RIU for the No. 3. Comparing the two types of microcavities, despite lower *d*, the U-shape microcavity may offer a slightly higher $S_{RI}$ in a given wavelength range, i.e., minima marked as No. 1 in Fig. 5. On the other hand, the V-trench structure offers an additional minimum in the examined wavelength range. This feature can be particularly useful as a supplementary verification of the measurement results and when the wavelength range of the interrogating setup is limited.

In Table 2 the $S_{RI}$ reported for μIMZI in the literature and those examined in this paper are compared. It can be found that the sensitivities shown in Fig. 5 for the two chosen shapes of the microcavities are among the highest published to date. It must be noted that with the increase of the RI other minima appear in the observed wavelength range, and the $S_{RI}$ increases. Moreover, high $S_{RI}$ and well-defined spectral patterns were achieved without additional post-processing, e.g., RIE or HF etching. It must be also noted that the V-trench microcavity is the only one from the list where due to high *d* three minima appear.

### 4.2. Application in microfluidic systems

The investigated medium needs to be delivered to the microcavity volume and later to its bottom to be investigated there. Filling the cavity with the medium is relatively easy in the case of gases. However, for liquids the procedure may not be that trivial and requires application of a low-volume pipette and some time to exchange the medium or a microfluidic system. The latter approach is favorable due to enhanced repeatability of the procedure and automatized washing capability.

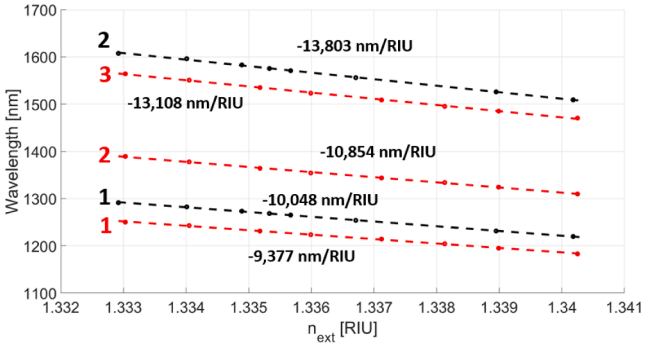


**Fig. 5.** Results of experimental analysis showing sensitivity of the U-shape (black lines) and V-trench (red lines) microcavities to changes in RI filling the microcavity ($n_{ext}$). The numbers next to the lines corresponds to the minimum order indicated in Fig. 4(A) and 4(B). (For interpretation of the references to colour in this figure legend, the reader is referred to the web version of this article.)

The results of numerical calculations of medium flow and concentration change at the bottom of the two shapes of the microcavities after the medium introduction are shown in Fig. 6. For the same cavity orientation versus the flow there is a significant difference in efficiency of the medium exchange which favors the U-shape. The Videos presenting the evolution of the exchange in time are available as Video 1 and 2 for U-shape and V-trench respectively. The exchange at the bottom of V-trench may be inefficient and requires significantly longer flushing time.

The influence of the orientation of the cavities versus the flow direction for both shapes has also been analyzed. As expected, the fluid exchange in the V-trench microcavity is much slower than in the U-shape one, Fig. 7(A). The fastest liquid exchange takes place when the microcavity is oriented perpendicularly to the liquid flow (Fig. 7(B)). The shape of the microcavity affects the total time of the fluid exchange but does not make it more advantageous to arrange the microcavity at a specific angle versus the flow. The results suggest that a U-shape microcavity would perform better in high speed microfluidic applications or automatized biosensing procedure. The analysis indicates that the replacement of the solution in narrow cavities is, in general, longer than for the wider ones.

## 5. Conclusions

In recent years, Mach-Zehnder interferometers based on optical fibers have attracted significant attention of scientific community dealing with sensors. The structures based on microcavities are of interest due to capability to analyze optical properties of low or very low volumes. Using precise material processing methods such as femtosecond laser micromachining, it is possible to control geometry of the microcavity in the optical fiber and thus meet different sensing requirements. In this work on top of review on reported microcavity shapes, the sensing performance of two exemplary interferometers based on U-shape and V-trench were analyzed experimentally and numerically. Their advantages and disadvantages from the application point of view were identified. While the interaction length between the core and the medium in the cavity mainly determines the sensitivity of the device to changes in refractive index filling the cavity, the microcavity shape has an impact on mechanical robustness of the structure and effectiveness of medium exchange in the cavity. While V-shape cavities along the fiber may offer mechanical robustness and flexibility in tuning optical response, more open cavities such as circular U-shape are more beneficial when microcavity washing is required, as it is in case of label-free biosensing, or installation of other supporting devices there, such as electrodes. Thus, depending on the application, which include medical, biological, chemical examinations different microcavity shapes should be chosen. The analysis shown in this work may be helpful in designing various microcavity-based devices for specific applications.

## CRediT authorship contribution statement

**Tomasz Gabler:** Data curation, Investigation, Writing – original draft, Writing – review & editing. **Monika Janik:** Data curation, Formal analysis, Writing – original draft. **Changrui Liao:** Formal analysis, Investigation. **Anna Myśliwiec:** Data curation, Investigation. **Marcin Koba:** Formal analysis, Methodology, Writing – original draft, Writing – review & editing. **Martin Jönsson-Niedziółka:** Data curation, Formal analysis, Investigation, Writing – original draft. **Ying Wang:** Formal analysis, Funding acquisition, Methodology, Resources, Supervision. **Mateusz Śmietana:** Conceptualization, Formal analysis, Funding acquisition, Methodology, Project administration, Resources, Software, Supervision, Writing – original draft, Writing – review & editing.

## Declaration of Competing Interest

The authors declare that they have no known competing financial

**Table 2**
RI sensing performance of μIMZIs compared for different shapes and manufacturing methods.

| Microcavity shape | $S_{RI}$ [nm/RIU]* | Minimum wavelength range [nm] | $n_{ext}$ [RIU] | Manufacturing method | Ref. |
|---|---|---|---|---|---|
| D-shape | −12,126 | 1500–1550 | 1.333–1.338 | Fs laser | [45] |
| Microcavity with microchannels | −10,055 | 1375–1650 | 1.305–1.330 | Fs laser, HF etching | [36] |
| Three embedded microchannels | −2,406 | 1500–1625 | 1.333–1.383 | Fs laser | [50] |
| V-shape | − 8,227 | 1500–1590 | 1.333–1.346 | Fs laser, HF etching | [46] |
| | − 10,537 | | | | |
| U-shape | −15,762 | 1250–1650 | 1.33–1.36 | Fs laser, RIE | [48] |
| | –23,345 | | 1.42–1.44 | | |
| U-shape | − 10,048 | 1250–1300 | 1.333–1.341 | Fs laser | This work |
| | − 13,802 | 1500–1600 | | | |
| V-trench | −9,377 | 1200–1250 | 1.333–1.341 | Fs laser | This work |
| | −10,854 | 1300–1400 | | | |
| | −13,108 | 1475–1575 | | | |

*If more than one value is given it indicates several minima observed.

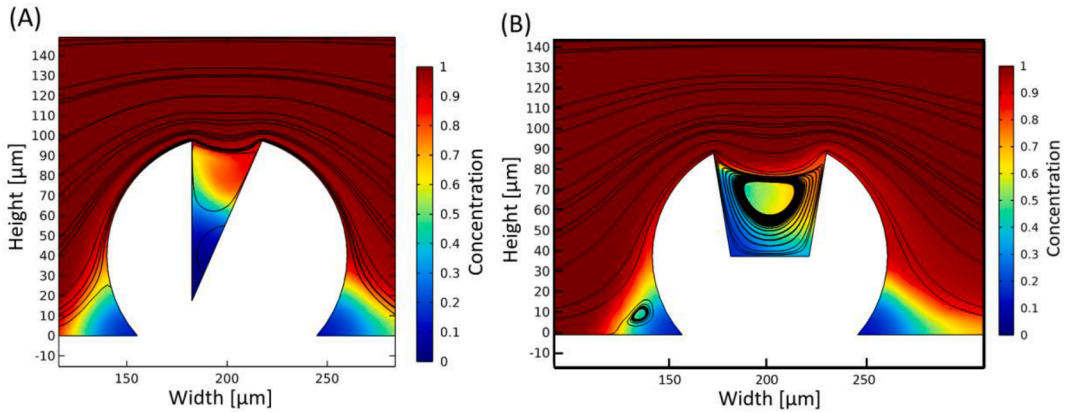


**Fig. 6.** (A) and (B) show results of simulation of streamlines and the liquid concentration at the 0.25 s and flow speed 25 μl/min for V-trench and U-shape microcavities, respectively.

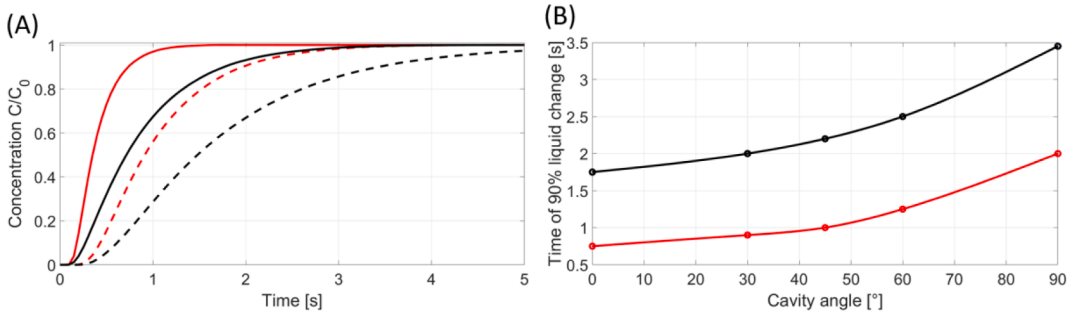


**Fig. 7.** (A) Results of simulation presenting concentration at the bottom of U-shape microcavity (solid lines) and the bottom of the V-trench microcavity (dashed lines). Red and black represent the angle of microcavity at $\theta = 0^\circ$ and $\theta = 90^\circ$ versus the flow direction, respectively, i.e., $\theta = 0^\circ$ indicates vertical cavity, and $\theta = 90^\circ$ indicates the cavity oriented towards the flow. (B) Calculated time required for 90% liquid exchange for the circular (red) and trench (black) microcavities at different orientations versus the flow.

interests or personal relationships that could have appeared to influence the work reported in this paper.

## Data availability

Data will be made available on request.

## Acknowledgements

This work was supported by the National Science Centre (NCN), Poland, under grant No. 2018/29/B/ST7/02552 and the internal grant of Warsaw University of Technology (Poland) supporting scientific activity in Automatics, Electronics and Electrotechnics received in 2020. M. Janik acknowledges the support from the Foundation for Polish Science within the START 2021 program. Support received from Piotr Szczerbetka within optical measurements is also acknowledged.

## Appendix A. Supplementary data

Supplementary data to this article can be found online at https://doi.org/10.1016/j.yofte.2022.103059.

## References

[1] M.S. Soares, et al., Immunosensing based on optical fiber technology: recent advances, *Biosensors* 11 (9) (2021), https://doi.org/10.3390/bios11090305.

[2] B. Kaur, S. Kumar, B.K. Kaushik, Recent advancements in optical biosensors for cancer detection, *Biosens. Bioelectron.* 197 (October 2021) (2022), 113805, https://doi.org/10.1016/j.bios.2021.113805.

[3] W. Xu, J. Liu, D. Song, C. Li, A. Zhu, F. Long, Rapid, label-free, and sensitive point-of-care testing of anti-SARS-CoV-2 IgM/IgG using all-fiber Fresnel reflection microfluidic biosensor, Microchim. Acta 188 (8) (2021).

[4] J. Li, Y. Liu, Y. Li, X. Li, J. Liang, S. Qu, Microfluidic volume optical monitoring system based on functional channels integrated by hollow cylindrical waveguide, Meas. J. Int. Meas. Confed. 193 (2022), 110951, https://doi.org/10.1016/j.measurement.2022.110951.

[5] P. Nag, K. Sadani, S. Mukherji, Optical fiber sensors for rapid screening of COVID-19, Trans. Indian Natl. Acad. Eng. 5 (2) (2020) 233–236, https://doi.org/10.1007/s41403-020-00128-4.

[6] S.M. Lee, M.Y. Jeong, S.S. Saini, Etched-core fiber Bragg grating sensors integrated with microfluidic channels, J. Light. Technol. 30 (8) (2012) 1025–1031, https://doi.org/10.1109/JLT.2011.2167220.

[7] J. Lim, G. Choi, K. Il Joo, H.J. Cha, J. Kim, Embolization of vascular malformations via in situ photocrosslinking of mechanically reinforced alginate microfibers using an optical-fiber-integrated microfluidic device, Adv. Mater. 33 (14) (2021) 1–9, https://doi.org/10.1002/adma.202006759.

[8] S.-C. Yan, F. Xu, A review on optical microfibers in fluidic applications, J. Micromech. Microeng. 27 (9) (2017) 093001.

[9] Y. Zhao, X.-G. Hu, S. Hu, Y. Peng, Applications of fiber-optic biochemical sensor in microfluidic chips: a review, Biosens. Bioelectron. 166 (2020) 112447.

[10] D. Wu, T. Zhu, M. Deng, D.-W. Duan, L.-L. Shi, J. Yao, Y.-J. Rao, Refractive index sensing based on Mach-Zehnder interferometer formed by three cascaded single-mode fiber tapers, Appl. Opt. 50 (11) (2011) 1548.

[11] Y. Geng, X. Li, X. Tan, Y. Deng, Y. Yu, High-sensitivity Mach-Zehnder interferometric temperature fiber sensor based on a Waist-Enlarged fusion bitaper, IEEE Sens. J. 11 (11) (2011) 2891–2894, https://doi.org/10.1109/JSEN.2011.2146769.

[12] B. Li, L. Jiang, S. Wang, L. Zhou, H. Xiao, T. Hai-Lung, Ultra-abrupt tapered fiber mach-zehnder interferometer sensors, Sensors 11 (6) (2011) 5729–5739, https://doi.org/10.3390/s110605729.

[13] C. Liao, F. Zhu, P. Zhou, Y. Wang, Fiber taper-based mach-zehnder interferometer for ethanol concentration measurement, Micromachines 10 (11) (2019) 1–7, https://doi.org/10.3390/mi10110741.

[14] Z. Tian, S.-H. Yam, J. Barnes, W. Bock, P. Greig, J.M. Fraser, H.-P. Loock, R. D. Oleschuk, Refractive index sensing with Mach-Zehnder interferometer based on concatenating two single-mode fiber tapers, IEEE Photonics Technol. Lett. 20 (8) (2008) 626–628.

[15] S. Gao, W. Zhang, H. Zhang, C. Zhang, Reconfigurable and ultra-sensitive in-line Mach-Zehnder interferometer based on the fusion of microfiber and microfluid, Appl. Phys. Lett. 106 (8) (2015) 084103.

[16] S. Marrujo-García, I. Hernández-Romano, D.A. May-Arrioja, V.P. Minkovich, M. Torres-Cisneros, In-line mach–zehnder interferometers based on a capillary hollow-core fiber using vernier effect for a highly sensitive temperature sensor, *Sensors* 21 (16) (2021), https://doi.org/10.3390/s21165471.

[17] H.Y. Choi, M.J. Kim, B.H. Lee, Compact all-fiber Mach-Zehnder interferometers formed in photonic crystal fiber, Opt. InfoBase Conf. Pap. 15 (9) (2007) 476–481.

[18] J. Wang, B. Liu, Y. Wu, Y. Mao, L. Zhao, T. Sun, T. Nan, Y. Han, Temperature insensitive fiber Fabry-Perot/Mach-Zehnder hybrid interferometer based on photonic crystal fiber for transverse load and refractive index measurement, Opt. Fiber Technol. 56 (2020) 102163, https://doi.org/10.1016/j.yofte.2020.102163.

[19] M. Smietana, D. Brabant, W.J. Bock, P. Mikulic, T. Eftimov, Refractive-index sensing with inline core-cladding intermodal interferometer based on silicon nitride nano-coated photonic crystal fiber, J. Light. Technol. 30 (8) (2012) 1185–1189, https://doi.org/10.1109/JLT.2011.2175201.

[20] F. Zhang, J. He, X. Xu, Y. Wang, "Highly sensitive temperature sensor based on a Mach-Zehnder interferometer created in graded index fiber," *Asia Commun. Photonics Conf. ACP*, 2018(10) 2018 2466–2469, doi: 10.1109/ACP.2018.8596293.

[21] R. Wang, J. Zhao, Y. Sun, H. Yu, N. Zhou, H. Zhang, D. Jia, Wearable respiration monitoring using an in-line few-mode fiber Mach-Zehnder interferometric sensor, Biomed. Opt. Express 11 (1) (2020) 316.

[22] Y.-J. Rao, Z.-L. Ran, Optic fiber sensors fabricated by laser-micromachining, Opt. Fiber Technol. 19 (6) (2013) 808–821.

[23] Y. Lei, H. Xiao, C. Chair John Ballato Liang Dong Lin Zhu, "Femtosecond Laser Micromachining of Advanced Fiber Optic Sensors and Devices," 2017.

[24] S.J. Mihailov, C.W. Smelser, P. Lu, R.B. Walker, D. Grobnic, H. Ding, G. Henderson, J. Unruh, Fiber Bragg gratings made with a phase mask and 800-nm femtosecond radiation Title, Opt. Lett. 28 (12) (2003) 995.

[25] A. Martinez, M. Dubov, I. Khrushchev, I. Bennion, Direct writing of fibre Bragg gratings by femtosecond laser, Electron. Lett. 40 (19) (2004) 1170–1172.

[26] X. Fang, C.R. Liao, D.N. Wang, Femtosecond laser fabricated fiber Bragg grating in microfiber for refractive index sensing, Opt. Lett. 35 (7) (2010) 1007, https://doi.org/10.1364/ol.35.001007.

[27] Y. Kondo, N. Kentaro, M. Tsuneo, W. Masaru, P. Kazansky, K. Hirao, Fabrication of long-period fiber gratings by focused irradiation of infrared femtosecond laser pulses, Opt. Lett. 24 (1999) 646–648, https://doi.org/10.1364/OL.24.000646.

[28] A. Theodosiou, R. Min, A.G. Leal-Junior, A. Ioannou, A. Frizera, M.J. Pontes, C. Marques, K. Kalli, Long period grating in a multimode cyclic transparent optical polymer fiber inscribed using a femtosecond laser, Opt. Lett. 44 (21) (2019) 5346.

[29] X. Sun, P. Huang, J. Zhao, L. Wei, N. Zhang, D. Kuang, X. Zhu, Characteristic control of long period fiber grating (LPFG) fabricated by infrared femtosecond laser, Front. Optoelectron. 5 (3) (2012) 334–340.

[30] T. Wei, Y. Han, H.-L. Tsai, H. Xiao, Miniaturized fiber inline Fabry-Perot interferometer fabricated with a femtosecond laser, Opt. Lett. 33 (2008) 536–538, https://doi.org/10.1364/OL.33.000536.

[31] T. Wei, Y. Han, H.-L. Tsai, H. Xiao, Miniaturized fiber inline Fabry-Pérot interferometer for chemical sensing, *Photonic Microdevices/Microstructures Sens.* 7322 (April 2009) (2009) 73220F, https://doi.org/10.1117/12.818612.

[32] M. Park, S. Lee, W. Ha, D.-K. Kim, W. Shin, I.-B. Sohn, K. Oh, Ultracompact intrinsic micro air-cavity fiber mach-zehnder interferometer, IEEE Photonics Technol. Lett. 21 (15) (2009) 1027–1029.

[33] L. Jiang, J. Yang, S. Wang, B. Li, M. Wang, Fiber Mach-Zehnder interferometer based on microcavities for high-temperature sensing with high sensitivity, Opt. Lett. 36 (19) (2011) 3753, https://doi.org/10.1364/ol.36.003753.

[34] T.Y. Hu, D.N. Wang, Optical fiber in-line Mach–Zehnder interferometer based on dual internal mirrors formed by a hollow sphere pair, Opt. Lett. 38 (16) (2013) 3036.

[35] W. Talataisong, D.N. Wang, R. Chitaree, C.R. Liao, C. Wang, High-pressure sensor based on fiber in-line Mach-Zehnder interferometer, 24th Int Conf. Opt. Fibre Sensors 9634 (2015) 96345B, https://doi.org/10.1117/12.2190520.

[36] Z. Li, C. Liao, D. Chen, J. Song, W. Jin, G.-D. Peng, F. Zhu, Y. Wang, J. He, Y. Wang, Label-free detection of bovine serum albumin based on an in-fiber Mach-Zehnder interferometric biosensor, Opt. Express 25 (15) (2017) 17105.

[37] N.N.S. Ojha, A. Kumar, N. Kumar, Post-fabrication refractive index sensitivity enhancement technique for single-fiber Mach-Zehnder interferometer, *Opt. Fiber Technol.* 54 (December 2019) (2020), 102118, https://doi.org/10.1016/j.yofte.2019.102118.

[38] P. Lu, L. Men, K. Sooley, Q. Chen, Tapered fiber Mach-Zehnder interferometer for simultaneous measurement of refractive index and temperature, Appl. Phys. Lett. 94 (13) (2009) 18–21, https://doi.org/10.1063/1.3115029.

[39] Y. Jung, S. Lee, B.H. Lee, K. Oh, Ultracompact in-line broadband Mach-Zehnder interferometer using a composite leaky hollow-optical-fiber waveguide, Opt. Lett. 33 (24) (2008) 2934, https://doi.org/10.1364/ol.33.002934.

[40] C.R. Liao, H.F. Chen, D.N. Wang, Ultracompact optical fiber sensor for refractive index and high-temperature measurement, J. Light. Technol. 32 (14) (2014) 2531–2535, https://doi.org/10.1109/JLT.2014.2328356.

[41] J. Liu, D.N. Wang, L. Zhang, Slightly tapered optical fiber with dual inner air-cavities for simultaneous refractive index and temperature measurement, J. Lightwave Technol. 34 (21) (2016) 4872–4876.

[42] C.R. Liao, Y. Wang, D.N. Wang, M.W. Yang, Fiber in-line Mach-Zehnder interferometer embedded in FBG for simultaneous refractive index and temperature measurement, IEEE Photonics Technol. Lett. 22 (22) (2010) 1686–1688, https://doi.org/10.1109/LPT.2010.2079924.

[43] M. Janik, M. Koba, K. Król, P. Mikulic, W. Bock, M. Śmietana, Combined long-period fiber grating and microcavity in-line mach–zehnder interferometer for refractive index measurements with limited cross-sensitivity, Sensors (Switzerland) 20 (8) (2020) 1–13, https://doi.org/10.3390/s20082431.

[44] L. Zhao, L. Jiang, S. Wang, H. Xiao, Y. Lu, H.L. Tsai, A high-quality Mach-Zehnder interferometer fiber sensor by femtosecond laser one-step processing, Sensors 11 (1) (2011) 54–61, https://doi.org/10.3390/s110100054.

[45] L. Jiang, L. Zhao, S. Wang, J. Yang, H. Xiao, Femtosecond laser fabricated all-optical fiber sensors with ultrahigh refractive index sensitivity: modeling and experiment, Opt. Express 19 (18) (2011) 17591, https://doi.org/10.1364/oe.19.017591.

[46] X. Sun, X. Dong, Y. Hu, H. Li, D. Chu, J. Zhou, C. Wang, Ji'an Duan, A robust high refractive index sensitivity fiber Mach-Zehnder interferometer fabricated by femtosecond laser machining and chemical etching, Sensors Actuators, A Phys. 230 (2015) 111–116.

[47] Y. Wang, M. Yang, D.N. Wang, S. Liu, P. Lu, Fiber in-line Mach-Zehnder interferometer Fabricated By Femtosecond Laser Micromachining for Refractive Index Measurement With High Sensitivity, J. Opt. Soc. Am. B 27 (3) (2010) 370–374, https://doi.org/10.1364/josab.27.000370.

[48] M. Janik, A.K. Mysliwiec, M. Koba, A. Celebanska, W.J. Bock, M. Smietana, Sensitivity pattern of femtosecond laser Micromachined and plasma-processed In-Fiber Mach-Zehnder interferometers, as applied to small-scale refractive index sensing, IEEE Sens. J. 17 (11) (2017) 3316–3322, https://doi.org/10.1109/JSEN.2017.2695544.

[49] M. Janik, M. Koba, W.J. Bock, M. Śmietana, Influence of the size of a micro-cavity fabricated in an optical fiber using the femtosecond laser in a form of in-line Mach-Zehnder interferometer on its refractive index sensitivity, *Electron Technol. Conf. 2016* 10175 (December 2016) (2016) 101750P, https://doi.org/10.1117/12.2260761.

[50] Y. Liu, S. Qu, Y. Li, Liquid refractive index sensor with three-cascaded microchannels in single-mode fiber fabricated by femtosecond laser-induced water breakdown, Appl. Phys. B Lasers Opt. 110 (4) (2013) 585–589, https://doi.org/10.1007/s00340-012-5296-y.

[51] X.-Y. Sun, D.-K. Chu, X.-R. Dong, Chu-Zhou, H.-T. Li, Luo-Zhi, Y.-W. Hu, J.-Y. Zhou, Cong-Wang, J.-A. Duan, Highly sensitive refractive index fiber inline Mach-Zehnder interferometer fabricated by femtosecond laser micromachining and chemical etching, Opt. Laser Technol. 77 (2016) 11–15.

[52] M. Janik, M. Koba, A. Celebańska, W.J. Bock, M. Śmietana, Sensing properties of micro-cavity in-line Mach-Zehnder interferometer enhanced by reactive ion etching, Opt. Laser Technol. 103 (2018) 260–266, https://doi.org/10.1016/j.optlastec.2018.01.045.

[53] M. Janik, T. Eftimov, M. Koba, M. Smietana, W.J. Bock, Tailoring Properties of Microcavity In-Line Mach-Zehnder interferometer by the Microcavity enlargement using femtosecond laser, J. Light. Technol. 37 (18) (2019) 4501–4506, https://doi.org/10.1109/JLT.2019.2907661.

[54] M. Śmietana, M. Janik, M. Koba, W.J. Bock, Transition between bulk and surface refractive index sensitivity of micro-cavity in-line Mach-Zehnder interferometer induced by thin film deposition, Opt. Express 25 (21) (2017) 26118, https://doi.org/10.1364/oe.25.026118.

[55] M. Janik, M. Koba, A. Celebańska, W.J. Bock, M. Śmietana, Live E. coli bacteria label-free sensing using a microcavity in-line Mach-Zehnder interferometer, Sci. Rep. 8 (1) (2018) 4–11, https://doi.org/10.1038/s41598-018-35647-2.

[56] M. Janik, E. Brzozowska, P. Czyszczoń, A. Celebańska, M. Koba, A. Gamian, W. J. Bock, M. Śmietana, Optical fiber aptasensor for label-free bacteria detection in small volumes, *Sens. Actuators* B Chem. 330 (2021), 129316, https://doi.org/10.1016/j.snb.2020.129316.

[57] T. Eftimov, M. Janik, M. Koba, M. Śmietana, P. Mikulic, W. Bock, Long-period gratings and Microcavity In-Line Mach Zehnder interferometers as highly sensitive optical fiber platforms for bacteria sensing, Sensors 20 (13) (2020) 3772, https://doi.org/10.3390/s20133772.

[58] M. Janik, S.V. Hamidi, M. Koba, J. Perreault, R. Walsh, W.J. Bock, M. Śmietana, Real-time isothermal DNA amplification monitoring in picoliter volumes using an optical fiber sensor, Lab Chip 21 (2) (2021) 397–404, https://doi.org/10.1039/d0lc01069c.

[59] Y. Wang, Y. Li, C. Liao, D.N. Wang, M. Yang, P. Lu, High-temperature sensing using miniaturized fiber in-line Mach-Zehnder interferometer, IEEE Photonics Technol. Lett. 22 (1) (2010) 39–41, https://doi.org/10.1109/LPT.2009.2035638.

[60] T. Gabler, A. Krześniak, M. Janik, A. Myśliwiec, M. Koba, J. Buczyńska, M. Jönsson-Niedziółka, M. Śmietana, Electrochemistry in an optical fiber microcavity - optical monitoring of electrochemical processes in picoliter volumes, Lab Chip 21 (14) (2021) 2763–2770.

[61] T. Eftimov, A. Arapova, M. Janik, W.J. Bock, Broad range bimodal microcavity in-line Mach-Zehnder interferometers, *Opt. Laser Technol.* 145 (April 2021) (2022), 107503, https://doi.org/10.1016/j.optlastec.2021.107503.

[62] P. Biswas, N. Basumallick, S. Bandyopadhyay, K. Dasgupta, A. Ghosh, S. Bandyopadhyay, Sensitivity enhancement of turn-around-point long period gratings by tuning initial coupling condition, IEEE Sens. J. 15 (2) (2015) 1240–1245, https://doi.org/10.1109/JSEN.2014.2361166.

[63] A. Krześniak, T. Gabler, M. Janik, M. Koba, M. Jönsson-Niedziółka, M. Śmietana, A microfluidic system for analysis of electrochemical processing using a highly sensitive optical fiber microcavity, Opt. Lasers Eng. 158 (June) (2022) 1–9, https://doi.org/10.1016/j.optlaseng.2022.107173.